Structural Stabilization and Functional Improvement of Horseradish Peroxidase upon Modification of Accessible Lysines: Experiments and Simulation

Navid Mogharrab,* Hedayatollah Ghourchian,* and Mehriar Amininasab†
*Laboratory of Microanalysis, Institute of Biochemistry and Biophysics, and †Department of Cell and Molecular Biology, Faculty of Science, University of Tehran, Tehran, Iran

ABSTRACT Horseradish peroxidase (HRP) is an important heme enzyme with enormous medical diagnostic, biosensing, and biotechnological applications. Thus, any improvement in the applicability and stability of the enzyme is potentially interesting. We previously reported that covalent attachment of an electron relay (anthraquinone 2-carboxylic acid) to the surface-exposed Lys residues successfully improves electron transfer properties of HRP. Here we investigated structural and functional consequences of this modification, which alters three accessible charged lysines (Lys-174, Lys-232, and Lys-241) to the hydrophobic anthraquinolysine residues. Thermal denaturation and thermoinactivation studies demonstrated that this kind of modification enhances the conformational and operational stability of HRP. The melting temperature increased 3°C and the catalytic efficiency enhanced by 80%. Fluorescence and circular dichroism investigations suggest that the modified HRP benefits from enhanced aromatic packing and more buried hydrophobic patches as compared to the native one. Molecular dynamics simulations showed that modification improves the accessibility of His-42 and the heme prosthetic group to the peroxide and aromatic substrates, respectively. Additionally, the hydrophobic patch, which functions as a binding site or trap for reducing aromatic substrates, is more extended in the modified enzyme. In summary, this modification produces a new derivative of HRP with enhanced electron transfer properties, catalytic efficiency, and stability for biotechnological applications.

INTRODUCTION

Horseradish peroxidase (HRP) is a member of the plant peroxidase superfamily originally extracted from horseradish (*Armoracia rusticana*) roots which catalyzes the oxidation of a broad range of substrates by hydrogen peroxide or by organic peroxides (1). Like other plant peroxidases, the catalytic process of HRP occurs through a multi-step reaction (1–3):

$$\text{HRP (resting state)} + H_2O_2 \rightarrow \text{Compound I} + H_2O \quad (1)$$

$$\text{Compound I} + AH_2 \rightarrow \text{Compound II} + AH^{*} \quad (2)$$

$$\text{Compound II} + AH_2 \rightarrow \text{HRP (resting state)} + AH^{*}. \quad (3)$$

The resting ferric enzyme first reacts with H_2O_2 to yield the first short-lived intermediate, called compound I, which consists of an oxyferryl iron ($Fe^{4+}=O$) and a porphyrin π-cation radical. In the next steps, compound I is subsequently reduced to the resting state of the enzyme by reactions with two reducing substrate molecules (AH_2).

HRP consists of more than 30 isozymes (4). The predominant form is isoenzyme C (HRP C), a monomeric glycoprotein with a molecular weight of ~44 kDa. The complete amino acid sequence of HRP was first determined by Welinder (5), but the major advances in our understanding of the structure and function of HRP were initiated by the successful production of recombinant enzyme (6). The enzyme has been characterized as a single polypeptide chain consisting of 308 residues, with an N-terminal residue blocked by pyroglutamate. It is heavily glycosylated (18% by mass) and contains a single protoporphyrin IX as a prosthetic group, two calcium ions, four disulfide bonds, and eight N-linked carbohydrate chains (5,7,8,9). Gajhede et al. reported the crystal structure of glycan-free recombinant HRP in 1997 (10). Since then, the three-dimensional (3D) structure of catalytic intermediates and several substrate complexes of HRP have also been reported and subjected to molecular dynamics (MD) simulations (11–21). These reports provide detailed descriptions of the structurally and catalytically important residues in HRP. Simulation studies suggest that the major access of H_2O_2 to the heme site is through a specific pathway with a fluctuating entry point, located between Phe-68 and Phe-142 (11). High resolution crystal structures of the oxidized intermediates of HRP confirm the importance of Arg-38 and His-42 for peroxide catalysis (1,14,22,23). X-ray crystallography and simulation studies indicate that the reducing substrate-binding site of HRP is a hydrophobic pocket provided by residues His-42, Phe-68, Gly-69, Ala-140, Pro-141, Phe-142, and Phe-179 and heme methyl C18, and substrate oxidation occurs at the exposed heme edge, a region comprising the heme methyl C18 and heme meso C20 protons (10,12,14,24).

HRP has achieved a prominent position in the pharmaceutical, chemical, and biotechnological industries (25). Methods improving the stability and functionality of HRP will clearly broaden the range of its present and future applications. In this regard, chemical modification of solvent-accessible reactive side chains has been frequently used to

Submitted July 12, 2006, and accepted for publication October 20, 2006.

Navid Mogharrab and Mehriar Amininasab contributed equally to this work.
Address reprint requests to H. Ghourchian, Tel.: 98-21-6640-8920; Fax: 98-21-6640-4680; E-mail: hadi@ibb.ut.ac.ir; or M. Amininasab, Tel.: 98-21-6111-2472; E-mail: amininasab@khayam.ut.ac.ir.

0006-3495/07/02/1192/12 $2.00
doi: 10.1529/biophysj.106.092858

redesign the enzyme stability and activity. Among the surface-located residues, Lys modification has succeeded in stabilizing a number of enzymes, including aminotransferase, α-amylase, trypsin, α-chymotrypsin, and HRP (26–29). Accordingly, most of the stabilized chemical derivatives of HRP reported to date have involved Lys modifications (30–41). Modification of HRP histidines with different pyrocarbonates had either neutral or negative effects on stability (42). Modifications targeted against the accessible side chains of tyrosine, arginine, aspartic, and glutamic acid failed to stabilize HRP (35). Chemical modification of lysines, ranging from the use of a cross-linker through attachment of polyethylene glycol to simple acetylation, has succeeded in stabilizing HRP to varying degrees (30–41).

Chemical modification of amino acid side chains has also been widely used to incorporate a variety of chemical groups, such as nongenetically encoded optical and biophysical probes, into proteins (43). In a recently published study, we successfully used this strategy to improve electron transfer properties of HRP. Covalent attachment of an electron relay (anthraquinone 2-carboxylic acid, AQ) to the surface-exposed Lys residues of HRP enabled the enzyme to exchange electrons directly with a conventional electrode (44). Here, we report experimental evidence indicating that the modification also enhances both the stability and catalytic efficiency of the enzyme. To clarify structural changes relating to stability enhancement, comparative studies between the native and AQ-modified HRP (AQ-HRP) were done using circular dichroism (CD) and fluorescence techniques. We have also performed MD simulations on native and AQ-HRP mainly to investigate structural and dynamical changes leading to the observed improvement in catalytic efficiency of the enzyme upon modification.

MATERIALS AND METHODS

Chemicals

HRP (donor: hydrogen peroxide, oxidoreductase, EC 1.11.1.7), sodium 4-(2-hydroxyethyl)-1-piperazineethansulfonate (Na-HEPES), AQ 98%, hydrogen peroxide 30% (w/w) solution, 4-aminoantipyrine 98% (4-AAP), 1-(3-dimethylaminopropyl)-3-ethyl carbodiimide hydrochloride 98% (DEC), ethylene-glycol bis(*N*-hydroxysuccinimidylsuccinate) (EGNHS), sodium dodecyl sulfate (SDS), 8-anilino-1-naphthalenesulfonic acid ammonium salt (ANS), and Nile Red (NR) were purchased from Sigma (St. Louis, MO). 2,4,6-Trinitrobenzene sulfonic acid (TNBSA) 1% (w/w) in *N,N*-dimethyl formamide was obtained from Fluka Chemie (Steinheim, Germany). Superfine Sephadex G-25 was supplied by Pharmacia LKB (Uppsala, Sweden). Phenol, potassium dihydrogen phosphate, dipotassium hydrogen phosphate, hydrogen chloride, and Coomassie brilliant blue G250 were purchased from Merck (Darmstadt, Germany). All reagents were commercially available and employed without further purification. Solutions and buffers were prepared using deionized double distilled water purified with an ultrapure water system (Nanopor Infinity, Barnstead, UK).

Preparation of the modified enzyme

Modification of HRP with AQ and EGNHS was performed according to the reported protocols (37,44). The enzyme concentration was determined using the Bradford method (45).

Determination of the extent of AQ modification

The average number of AQ-modified amino groups in HRP was determined following the method described by Habeeb (46,47), where the protein is unfolded in the procedure by HCl and SDS, and thus all amino groups are solvent accessible in the test. Briefly, the native and AQ-modified HRP were serially dissolved in 0.5 ml of 0.1 M sodium bicarbonate buffer (pH 8.85) to achieve concentrations of 0.1–0.8 mg/ml. To these solutions and buffer blanks 0.25 ml of 0.01% TNBSA (w/v) was added and mixed well. The reaction mixtures were incubated at 37°C for 2 h. At this point, 0.25 ml of 10% SDS solution (w/v) and 0.125 ml of 1 M HCl were added and their absorbance was measured at 335 nm using 1-cm path length quartz cuvettes. Absorbance values were plotted versus the protein concentration. The average number of AQ molecules per HRP molecule (n) was calculated from the following expression:

$$n = \left(1 - \frac{\text{slope of AQ-HRP plot}}{\text{slope of HRP plot}}\right) \times 6. \quad (4)$$

The multiplicative factor 6 is the number of free primary amines in HRP.

Enzyme assay

The activities of the native and modified enzymes were determined colorimetrically, using phenol, 4-AAP, and H_2O_2 as the dye-generating compounds (48). The reaction rate was determined by measuring the increases in absorbance at 510 nm resulting from the formation of a colored compound, *N*-antipyryl-*p*-benzoquinoneimine. One unit of activity results in the decomposition of one micromole of hydrogen peroxide per minute at 25°C and pH 7.0. Spectroscopic measurements were carried out in potassium phosphate buffer (0.2 M, pH 7.0) at 25°C using an ultraviolet (UV)-visible spectrophotometer (Cary 100 bio, Varian, Mulgrave, Victoria, Australia) equipped with a temperature controller.

Characterization of transition states

The effect of temperature on the rate of enzymatic reaction was determined over a temperature range of 10–85°C in 0.2 M potassium phosphate buffer, pH 7.0. At each temperature, the reaction mixture (total volume of 970 μL), including all reagents necessary for a substrate-saturated assay except the enzyme was first incubated in spectrophotometer for 5 min to achieve thermal equilibration. The enzyme solution (30 μL) was then added and the initial activity of the enzyme (the rate constant, k_{cat}) was immediately determined for the first 10 s. Such a short period was chosen to minimize the denaturation of enzyme at high temperatures during activity measurements.

The Arrhenius plots constructed from experimentally determined k_{cat} values in the temperature range of 15–60°C were used to calculate the activation energies (E_a) as follows (49):

$$E_a\,(\text{J mol}^{-1}) = -R \times (\text{slope of the Arrhenius plot}), \quad (5)$$

where R is the universal gas constant (8.31434 J mol^{-1} K^{-1}). The free energy of activation ($\Delta G^{\#}$) was determined by linear regression analysis of the Eyring plot, $\ln(k_{cat}/T)$ versus $1/T$, as follows:

$$\Delta G^{\#}\,(\text{J mol}^{-1}) = -R \times (\text{slope of the Eyring plot}). \quad (6)$$

The activation enthalpy ($\Delta H^{\#}$) and entropy ($\Delta S^{\#}$) at temperature T were calculated using the equations

$$\Delta H^{\#}\,(\text{J mol}^{-1}) = E_a - RT \quad (7)$$

$$\Delta S\,(\text{J mol}^{-1}\,\text{K}^{-1}) = \frac{\Delta H^{\#} - \Delta G^{\#}}{T}. \quad (8)$$

Irreversible thermoinactivation

The time course of irreversible thermoinactivation was studied by incubating the enzyme (native or modified) at 1.0 mg/ml concentration in 0.2 M potassium phosphate buffer, pH 7.0, at the desired temperature. At regular intervals, samples were removed and cooled on ice, and the remaining activity was determined as described above. Activity of the same enzyme solution kept on ice was considered as the control.

Electrochemical measurements

Electrochemical measurements were performed according to the reported procedure (44).

Circular dichroism measurements

CD measurements were performed on an Aviv Model 215 Circular Dichroism Spectrometer (Lakewood, NJ) at 25°C, using rectangular quartz cells with a path length of 1.0 mm for far-UV and 10 mm for near-UV and Soret spectra. The protein concentration in the samples was 10 μM for far-UV and 20 μM for near-UV and Soret CD, in 0.2 M potassium phosphate buffer, pH 7.0. Spectra were recorded with a wavelength step of 1 nm and an averaging time of 1 s. Each spectrum was an average of five continuous scans, corrected by subtracting the appropriate blank runs on HRP-free solutions and subjected to a moderate degree of noise-reduction analysis.

Temperature dependences of ellipticity at 222 nm were recorded under the same condition as far-UV-CD in the temperature range of 25–100°C with the constant heating rate of 1 K min^{-1}.

Fluorescence measurements

Intrinsic, ANS-, and NR-binding fluorescence spectra of the proteins were measured at 25°C using a Varian Cary Eclipse fluorescence spectrophotometer with the excitation and emission slit widths of 5 nm. Fluorescence emission from Trp was measured using excitation at 295 nm to avoid the contribution of tyrosines. In intrinsic fluorescence studies, the concentration of protein was 11.36 μM in 0.2 M potassium phosphate buffer, pH 7.0. For ANS-binding fluorescence, the excitation wavelength was 350 nm, and each sample contained 5.68 μM protein and 565 μM ANS in aqueous buffer. To study NR-binding fluorescence, the excitation wavelength was set to 530 nm and measurements were taken using samples with final concentrations of 23 μM protein and 2.0 μM NR.

Molecular dynamics simulations

All MD simulations were carried out using the GROMACS simulation package (50–52), version 3.2 with GROMACS force field, on an Intel Dual Xeon PC workstation under Red Hat Linux 9.0. The starting atomic coordinate of native HRP was obtained from Protein Data Bank (PDB) code 1ATJ (10). The GROMACS topology and parameter files of Aql (AQ-modified Lys residue) were generated using PRODRG web server (53,54). Then, the Lys side-chain residues 174, 232, and 241 of native HRP were modified to Aql to generate the initial structure of AQ-HRP. Each protein, native or modified HRP, was centered in a cubic box and then solvated with water molecules. The dimensions of the simulation box were chosen large enough to include at least 0.8 nm of solvent on each side of the protein molecule. Counterions Cl^- and Na^+ were added by replacing water molecules at random positions to achieve a neutral simulation box. The solvated and neutralized system was subjected to energy minimization until the maximum force was smaller than 500. In all simulations, the temperature and pressure were kept close to 300 K and 1 bar, respectively, by the Berendsen algorithm (55), with $\tau_T = 0.1$ ps and $\tau_P = 0.5$ ps. Bond lengths were constrained using the LINCS algorithm (56). Lennard-Jones and short-range electrostatic interactions were calculated with 1.0- and 1.4-nm cutoffs, respectively, and a particle mesh Ewald algorithm was used for the long-range electrostatic interactions (57). The neighbor list was updated every 10 steps. Each component of the system was coupled separately to a thermal bath, and isotropic pressure coupling was used to keep the pressure at the desired value. A time step of 2 fs was used for the integration of equation of motion. To relax the solvent molecules, a 20-ps position-restrained MD simulation was preformed to equilibrate the system. Then, a 100-ps equilibration without position restraints was applied. Finally, the production MD period of 5000 and 10,000 ps at constant pressure and temperature was performed on native and AQ-HRP, respectively.

RESULTS

Experimental results

Chemical modification of the enzyme

It has been reported that carbodiimide is an effective agent for coupling primary amines and carboxylic acids to make amides (58). Native HRP contains six Lys residues, plus a buried *N*-terminal α-amino group, which is blocked by the pyrrolidone carboxylic acid and unable to react with the coupling reagents. Thus, native HRP contains six potential primary amines to be coupled with the carboxylic acid group of AQ molecules (5). After modification, any reacting lysyl residue is altered to Aql, an artificial amino acid in which the ε-nitrogen of the Lys side chain is in amide linkage to the carbonyl group of AQ. Unlike the positively charged lysyl residue, Aql has a neutral bulky hydrophobic side chain. Hence, this modification changes the hydrophobic profile and charge distribution at the protein surface. By targeting the free ε-amino groups of Lys residues, the carbohydrate portions of HRP remain intact for further modification or immobilization of the enzyme.

Native and AQ-modified HRP were treated with TNBSA to determine their intact Lys contents. From the total of six lysyl residues, the average number of modified ones was determined to be 3 ± 0.5. Analysis of the side-chain accessibility and ε-amino surface area of lysines in HRP indicate that only the side-chain ε-nitrogens of Lys-174, Lys-232, and Lys-241 are well accessible and thus prone to react with modifiers. To validate this prediction, O'Brien et al. used proteolytic fragmentation, peptide sequencing, and mass spectrometry to identify the location of modified lysyl residues in chemically stabilized HRP (37). All three methods showed that HRP modification with the bifunctional compound EGNHS leads to complete modification of Lys-232, partial modification of Lys-174 and Lys-241, and very little reaction of Lys-65, Lys-84, and Lys-149.

To identify the sites of AQ modification, we used AQ as the reporter group and EGNHS to block the above specified Lys residues (37). HRP has only one Trp residue (Trp-117) located between two α-helixes at the side opposite the entrance to the heme-binding pocket. When excited at 295 nm, native HRP shows a typical Trp fluorescence emission spectrum, with a peak at 335 nm (Fig. 1 *A*). After modification, the

emission spectrum undergoes a drastic decrease in intensity and a blue shift to 330 nm. The observed blue shift (5 nm) in Trp fluorescence reflects reduced accessibility of Trp to the bulk solvent. As seen in Fig. 1 *A* (*inset*), AQ exhibits a significant absorption band centered at 330 nm, which closely overlaps the emission band of Trp-117. Therefore, in AQ-HRP, Trp emission is strongly quenched through the energy transfer to the attached AQ molecules. Moreover, AQ has a characteristic cyclic voltammogram, which makes it a useful labeling agent (44,59). Thus, any attached AQ molecule could be detected by both the fluorescence and cyclic voltammetry.

Native HRP was first modified with EGNHS to block the Lys residues 174, 232, and 241 (37). The average number of EGNHS-modified Lys residues per HRP molecule was determined by the TNBSA method to be 3.2 ± 0.3. The EGNHS-modified enzyme was then treated with AQ and DEC to modify any remaining free amino groups of accessible Lys residues. As seen in Fig. 1 *A*, whereas the Trp emission in AQ-HRP was drastically quenched, the enzyme which had undergone both modifications (EQ-HRP) showed an emission profile similar to that of native and EGNHS-modified HRP. In agreement, AQ-HRP exhibited the characteristic cyclic voltammogram of free AQ molecules with a reasonable shift, but no redox peak was detectable for EQ-HRP (Fig. 1 *B*). These observations indicate that no significant AQ attachment has occurred after the first modification; therefore, AQ molecules react mainly with the same residues as EGNHS.

Structural stability

In an attempt to evaluate how the modification affects the enzyme stability, we carried out a comparative thermal denaturation study by monitoring the loss of enzyme secondary structure at increasing temperatures. Thermal denaturation of HRP has been found to be irreversible and strongly scan rate dependent, indicating clearly that the denaturation process of this enzyme is kinetically controlled (60). Thus, it is difficult to obtain any thermodynamic information about the denaturation process because the kinetic effect interferes with them. Nevertheless, in such cases the apparent melting temperature (T_m) at a constant scan rate can be used for evaluation of enzyme stability as a function of experimental conditions.

Thermal denaturation of native and AQ-modified HRP was investigated by following the molar ellipticity [θ] at 222 nm as a function of temperature (Fig. 2). In both cases, denaturation of the enzyme was accompanied by an increase in molar ellipticity, and temperature-dependence pattern of molar ellipticity indicated a two-state melting of the secondary structure with a single cooperative transition between the native and denatured forms of the enzyme. T_m values were calculated from the first order derivative of ellipticity-temperature plots to be 72°C for native and 75°C for modified HRP. Thus, the T_m of modified HRP is 3°C higher than that of the native one, suggesting an improvement in conformational stability of the protein upon modification.

Operational stability

Operational stability of the native and modified forms of HRP was examined at 50°C and 70°C, pH 7.0. As shown in Fig. 3, upon incubation at 50°C, no significant difference between the native and modified HRP was observed, but modification resulted in a considerable enhancement in operational stability of the enzyme at 70°C. After 10-min incubation at 70°C, whereas the native HRP lost up to 96.4% of its initial activity, the lost activity of the modified HRP was $< 40\%$. To further investigate the structural changes contributing to stability enhancement, we performed comparative studies between the native and modified HRP using CD and fluorescence techniques.

Circular dichroism studies

The effect of AQ modification on the secondary and tertiary structure of HRP was investigated by near- and far-UV-CD. In the far-UV, the peptide bond is the principal absorbing group and studies in this region can give information on the secondary structure (61). Fig. 4 *A* shows the far-UV-CD spectra of native and AQ-modified HRP. For both proteins, the spectrum was characterized by a negative band with double minima at 208 and 222 nm, indicative of proteins with high contents of α-helical structure. Upon modification, the overall shape of the spectrum did not change significantly, but the intensity of the negative band increased. A

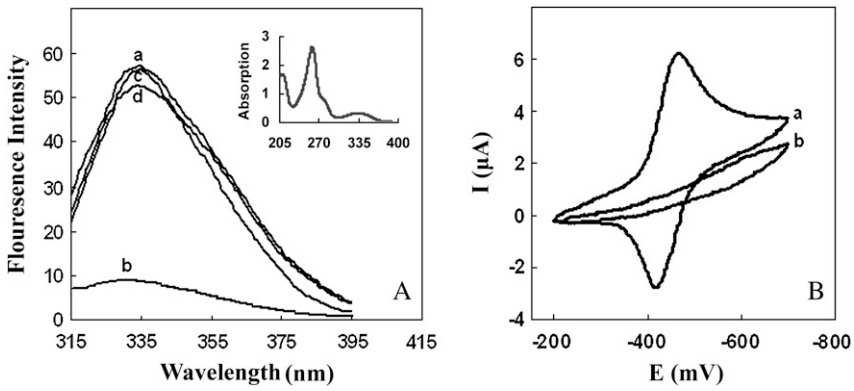

FIGURE 1 (*A*) Trp emission fluorescence spectra of native (*a*), AQ-HRP (*b*), EGNHS-HRP (*c*), and EQ-HRP (*d*) in a 0.2 M potassium phosphate buffer (pH 7.0) at 25°C. In all cases the enzyme concentration was 12 μM and the excitation wavelength was 295 nm. (*Inset*) Absorption spectrum of AQ in the same experimental conditions. (*B*) Cyclic voltammograms of AQ-HRP (*a*) and EQ-HRP (*b*) solutions in a 0.2 M potassium phosphate buffer (pH 7.0).

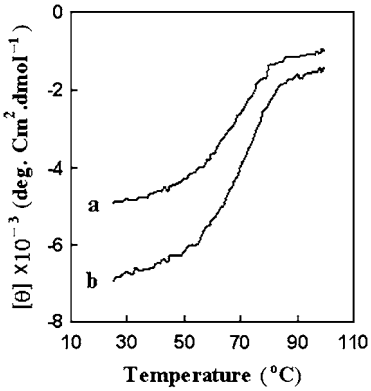

FIGURE 2 Temperature dependences of molar ellipticity at 222 nm for native (*a*) and AQ-modified HRP (*b*) in a 0.2 M potassium phosphate buffer (pH 7.0) obtained on heating with a constant scan rate of 1 K min $^{-1}$.

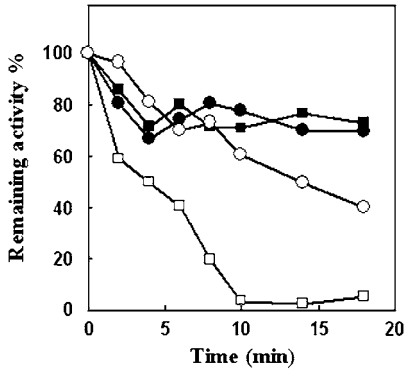

FIGURE 3 Irreversible thermoinactivation of native (*squares*) and modified (*circles*) forms of HRP determined at 50°C (*solid symbols*) and 70°C (*open symbols*), pH 7.0. Standard deviations were within 4% of the experimental values.

plausible interpretation for this observation is that the modified enzyme may benefit from higher α-helical content. However, this conclusion seems doubtful once we consider that the modified enzyme also contains three more amide bonds in its covalent structure, which could contribute to any far-UV absorption. So, at this stage, we are unable to make a clear judgment about the origin of the observed change in the far-UV-CD spectra.

CD spectra of native and modified HRP in near-UV (260–360 nm) and Soret (360–460 nm) regions are shown in Fig. 4 *B*. In the near-UV region, CD spectra of proteins reflect mainly the contribution of aromatic amino acids and disulfide bonds to protein tertiary structure and are very sensitive to structural perturbations (61). The near-UV-CD spectrum of HRP was characterized by a strong negative band centered at 284 nm, which is attributable to the presence of Trp and Tyr in asymmetric environments. In the case of modified HRP, this bond was more intense as compared with that of the native one, indicating enhanced aromatic packing after modification.

CD at the Soret region was monitored to find out the effect of modification on the heme active site. Changes in the Soret CD are related to the interaction of the heme prosthetic group with the surrounding aromatic residues and to modifications in the spatial orientation of these amino acids with respect to heme (62). These modifications affect porphyrin transitions and $\pi-\pi^*$ transitions in the surrounding aromatic residues. However, the protein-induced heme distortions from planarity and the contributions of polarizable groups (near the heme) have been postulated to participate to the ellipticity in the Soret region (63). Soret CD spectra of HRP exhibited a strong positive band at 407 nm. Again, comparison of the spectra showed higher intensity for AQ-HRP, indicating higher integrity of the heme pocket.

Fluorescence studies

The solvent exposure of hydrophobic patches in HRP was explored through ANS^- binding. ANS^- is a fluorescent hydrophobic probe that has been widely used to measure protein surface hydrophobicity. Fig. 5 *A* depicts the ANS^--binding profiles of the native and modified HRP. The fluorescence emission of ANS^- associated with modified HRP showed a reduced intensity and a red shift from 490 nm to 505 nm, as compared with that of the native one. Both changes reflect a

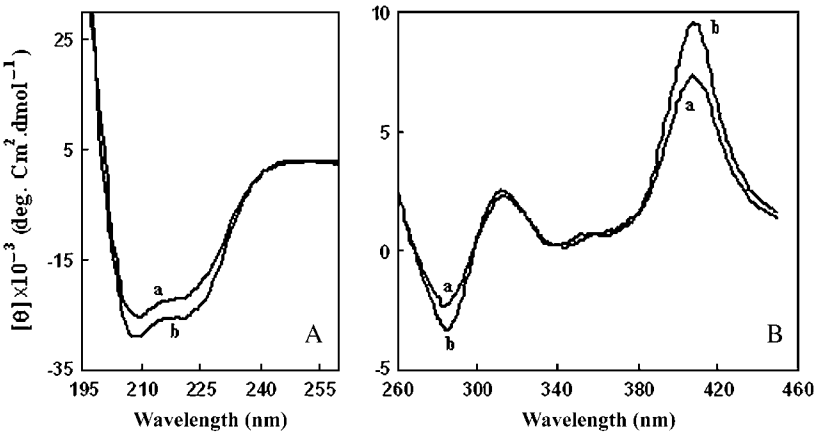

FIGURE 4 (*A*) Far-UV-CD spectra of 10 μM HRP. (*B*) Near-UV and Soret CD spectra of 20 μM HRP. *a* and *b* refer to the native and AQ-modified HRP, respectively. In these measurements, the enzyme was dissolved in a 0.2 M potassium phosphate buffer (pH 7.0) and the temperature was set to 25°C.

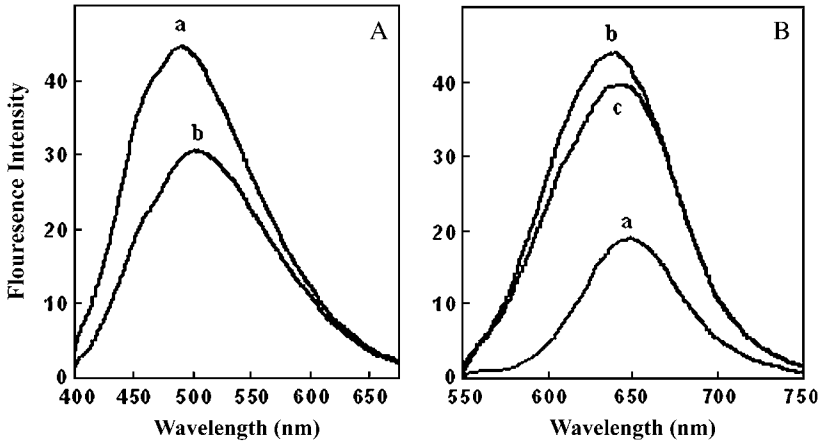

FIGURE 5 (*A*) Fluorescence emission spectra of ANS in the presence of native (*a*) and AQ-modified HRP (*b*) at 25°C. The excitation wavelength was 350 nm, and each sample contained 5.68 μM protein and 565 μM ANS in 0.2 M potassium phosphate buffer (pH 7.0). (*B*) Fluorescence emission spectra of NR alone in aqueous buffer (*a*), NR in the presence of 23 μM native (*b*), and AQ-modified HRP (*c*). The excitation wavelength was set to 530 nm and measurements were taken using samples with final concentration of 2.0 μM NR. All spectra were obtained at 25°C in 0.2 M potassium phosphate buffer (pH 7.0).

modification-induced conformational change leading to a decrease in the number of binding sites for ANS^- molecules. However, because ANS^- is an anion bearing a sulfonate (SO_3^-) group, it also can bind to the positively charged groups on the protein surface through ion pair formation. Recent studies have shown that ANS^- binding to proteins depends primarily on protein cationic charge and occurs largely through the ANS^- sulfonate group, but after binding, ANS^- fluorescence depends on a tangle of properties, including the polarity of its microenvironment. In fact, the range of ANS^- binding over which ANS^- produces its brilliant fluorescence generally is far narrower than the overall range of ANS^- binding set by electrostatic forces; for example, it has been reported that only 5 out of ~100 ANS^- anions bound to bovine serum albumin exhibit strong fluorescence production (64). In the case of AQ-HRP, the positive charges of modified Lys residues are lost after modification and thus decreasing the number of surface charges lessens the number of prone electrostatic sites for ANS^- binding. Consequently, neutralization of positive charges on Lys residues upon modification may contribute to the observed reduction in ANS^- fluorescence intensity. Another concern with using ANS^- is that the absorption spectrum of ANS^- overlaps with that of AQ and heme. Thereby, AQ and heme molecules compete with ANS^- molecules in absorbing light. This effect also tends to reduce the quantum yield of ANS^- fluorescence.

To clarify these obscurities, we used NR as a polarity-sensitive fluorescent probe (65). This dye is an uncharged hydrophobic molecule whose high excitation wavelength solves the problems of absorption interference with Trp, AQ, and heme. Fig. 5 *B* illustrates the interaction of NR with native and modified HRP. In agreement with ANS^--binding studies, fluorescence of NR bound to AQ-HRP showed reduced emission intensity and an 8-nm red shift to 644 nm, indicating increased hydrophobic surface burial. Nevertheless, the extent of the observed decrease in fluorescence emission for NR binding was less than that of ANS^- binding, emphasizing the role of positive charge neutralization in overestimating the reduced surface hydrophobicity.

Taken together, the conclusion is reached that by using ANS/NR as a probe the overall accessible size of hydrophobic patches in AQ-HRP has been reduced.

Catalytic efficiency

As depicted in Table 1, AQ modification of HRP results in some measurable beneficial changes in the kinetic parameters of the enzyme. Upon modification, an increase of ~33% in the maximum velocity (V_{max}) and turnover number (k_{cat}) of the enzyme was observed. Also the K_m value decreased 26.3%, reflecting higher affinity of the AQ-HRP for its substrate. This may also be attributed to the enhancement of substrate-enzyme complex stability (66). Among the kinetic parameters, the 80% increase in catalytic efficiency (k_{cat}/K_m) of modified HRP, as compared with the native enzyme, is especially noticeable (see Table 1).

Temperature dependence of the enzymatic reaction kinetics

Like nonenzymatic reactions, enzyme activity increases by raising the temperature. Any change in the reactant species, including the enzyme, could alter the reaction rate. To explore the effect of AQ modification on temperature dependence of

TABLE 1 Kinetic and activation parameters for the enzymatic reaction of native and AQ-modified HRP

	K_m (mM)	V_{max} (U/mg)	k_{cat} (s^{-1})	k_{cat}/K_m ($s^{-1}mM^{-1}$)	Ea (kJ/mol)	$\Delta H^{\#}$ (kJ/mol)	$\Delta G^{\#}$ (kJ/mol)	$\Delta S^{\#}$ (J/mol K)
Native HRP	0.396 ± 0.040	455 ± 15	334 ± 11	843	40.7 ± 1.2	38.2 ± 1.2	38.1 ± 1.9	0.38
Modified HRP	0.292 ± 0.030	604 ± 19	443 ± 15	1517	36.3 ± 1.5	33.8 ± 1.5	33.7 ± 1.7	0.23

Thermodynamic activation parameters for the native and AQ-modified HRP at 25°C deduced from Arrhenius plots over the temperature range of 15–60°C.

reaction rate, initial enzyme activity was determined over the range of 10–85°C. The overall temperature activity pattern of native and modified HRP was similar, and in both cases the reaction rate increases up to 70°C but vanishes at higher temperatures (data not shown). This maximum is not the optimum temperature for enzyme activity because after a few minutes incubation at any temperature above 50°C, the reaction rate diminishes due to destabilization of the enzyme structure.

Arrhenius plots for the maximum activity of native and modified HRP were prepared in the temperature ranges of 15–60°C. Both plots were linear over this temperature range and give activation values summarized in Table 1. The linearity of the Arrhenius plots indicates that there is no change in the rate-determining steps of catalytic reactions over this temperature range. Analysis of the thermodynamic activation parameters at 25°C (Table 1) showed that upon chemical modification, the activation-free energy ($\Delta G^{\#}$) of the enzyme has decreased by 4.4 kJ mol^{-1}. The lower Gibbs-free energy of activation, $\Delta G^{\#}$, of AQ-HRP can be depicted as a lower energy barrier that has to be mastered by the ground-state enzyme-substrate complex ES to reach the activated state ES$^{\#}$ to react, therefore corresponding to higher activity. This is also in accordance with the 80% increase in k_{cat}/K_m of modified HRP relative to the native one. Furthermore, Table 1 shows that the main reason for the increased catalytic activity of modified HRP is the lower enthalpic contribution, $\Delta H^{\#}$, to the free energy of activation and the change of $\Delta S^{\#}$ upon modification is negligible. Lower $\Delta H^{\#}$ value may translate a reduced number of enthalpy-driven interactions that are broken in the ES complex before reaching the activated state, ES$^{\#}$.

SIMULATION RESULTS

General structural properties

Using the known x-ray crystallographic structure of the resting form of HRP C, two 3D models of HRP C were constructed differing in the residues 174, 232, and 241 (Fig. 6). Conserving the original amino acid pattern of the x-ray structure, the control model (n-HRP) was constructed with these residues to be lysines in their cationic forms. In the second model (AQ-HRP) the residues 174, 232, and 241 were replaced by Aql. The backbone root mean-square deviation (RMSD) of n-HRP and AQ-HRP structures relative to their own starting structures were 1.65 ± 0.3 and 1.36 ± 0.2 Å, respectively. These low RMSD values indicate that the MD runs were stable and the protein atoms did not significantly deviate from the starting structures during the MD simulations. The backbone RMSD also reflects the dynamics of the protein matrix. Average RMSD of AQ-HRP is lower than that of the native one and indicates a decreased flexibility of the protein backbone as a result of AQ modification. This conclusion is in line with the experimental results obtained by CD. The stability of the fluctuation of the total energy was also examined by calculating the ratio between the variance of total energy and the average energy. For all models, this ratio did not exceed 0.0008, thus showing that energy was conserved during the simulations and that the models were well equilibrated.

To provide a more detailed description of the mobility of the protein residues, the backbone RMSD per residue for native and modified HRP averaged in the course of simulation, along with per residue B-factor of the original crystallographic structure of HRP C (PDB code 1ATJ) are shown in Fig. 7. The gray bands indicate the helix and strand regions of HRP according to the crystallographic structure. Thirteen α-helices dominate the structure: 14–28 (*A*), 32–44 (*B*), 77–90 (*C*), 97–111 (*D*), 131–137 (*D′*), 145–153 (*E*), 160–171 (*F*), 181–185 (*F′*), 199–208 (*F′′*), 232–238 (*G*), 245–252 (*H*), 260–267 (*I*), and 270–284 (*J*). Two short antiparallel β-strands, 174–176 (β1) and 218–220 (β2), flank the large plant peroxidase insert between helices F and G. It is clear from this representation that residues located in structurally important regions mainly experience sensible reduction in their mobility upon modification. In particular,

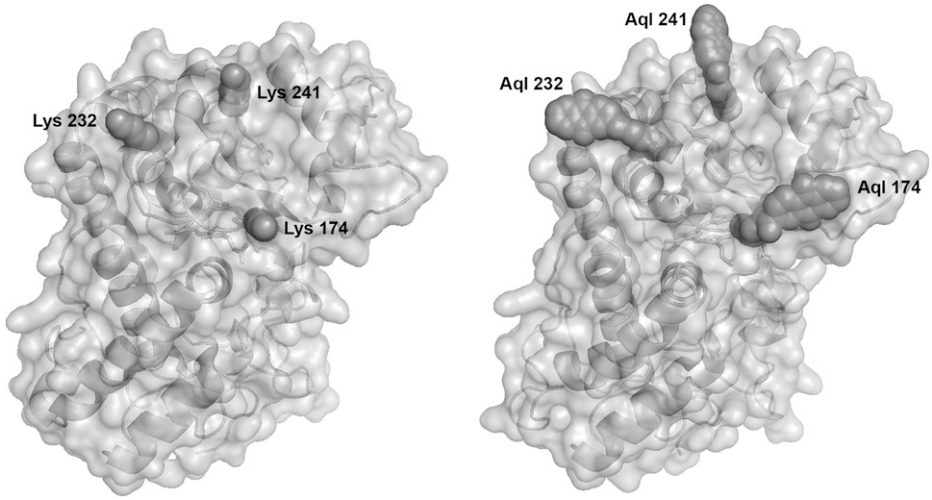

FIGURE 6 3D representation of the MD average structure of n-HRP (*left*) and AQ-HRP (*right*). The molecular surfaces are rendered in transparent light gray to make the ribbon models visible. Accessible Lys residues in n-HRP that are prone to modification and their counterpart Aql residues in AQ-HRP are shown in dark gray.

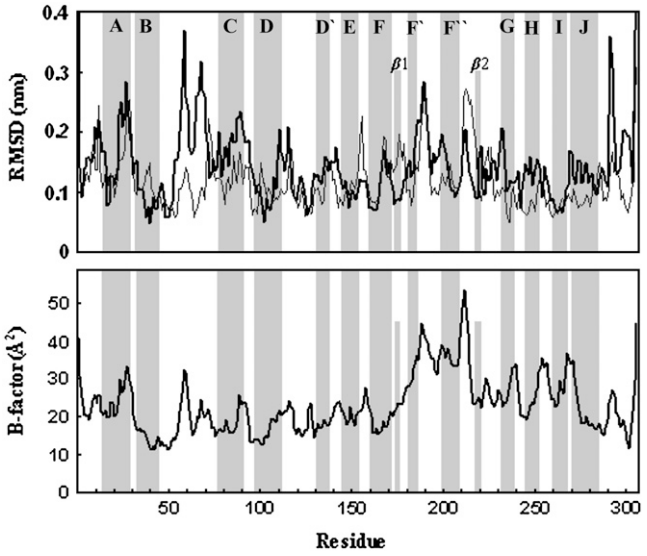

FIGURE 7 (*Top panel*) Backbone RMSD per residue for n-HRP (*bold black line*) and AQ-HRP (*gray line*). (*Bottom panel*) Backbone B-factor per residue of the original crystallographic structure (PDB code 1ATJ). The gray bands indicate the helix regions of HRP according to the crystallographic structure.

the helices A, C, D′, F′, G, H, and J, as well as the C-terminal residues show reduced mobility after modification. The connecting loops BC, CD, DD′, D′E, F′F′′, GH, HI, IJ, and the modified Lys residues 232 and 241 also demonstrate similar behavior. On the other hand, some parts of the protein structure including the helix B, the strand β1, and the connecting loops EF, Fβ1, and F′′β2 became more flexible upon modification. From all these graphics, again it is evident that AQ modification makes the overall backbone structure of the enzyme less flexible.

To evaluate the effect of conversion of three positively charged lysine residues to a hydrophobic one (Aql) on overall accessible hydrophobic area, the water accessibility of hydrophobic surface area in n-HRP and AQ-HRP was measured and averaged over the course of simulation. Interestingly, the overall water accessible hydrophobic area of modified HRP (76.4 nm^2) was more or less similar to the native one (75.9 nm^2). This indicates that in response to the introduction of three bulky hydrophobic residues, the protein readjusts itself to compensate the imposed surface hydrophobicity. This is achieved by the additional burial of some hydrophobic residues including Leu-208, Val-235, Leu-223, Leu-111, Cys-11, Ile-287, Ala-217, Phe-142, Pro-210, Cys-91, Leu-127, Leu-218, Ile-32, Ile-17, Leu-237, Trp-117, Phe-61, Leu-299, Ala-267, Phe-221, Gly-207, Ile-103, Phe-45, Met-281, Met-284, Met-181, Ala-276, Ala-129, Val-219, Leu-205, Ala-105, Gly-122, Pro-146, Leu-290, Leu-39, Gly-242, and Leu-37.

Peroxide-binding site

HRP catalyzes the oxidation of a broad range of organic (aromatic) and inorganic substrates by hydrogen peroxide or by organic peroxides. The main overall reaction catalyzed by HRP can be summarized as $H_2O_2 + 2\ AH \rightarrow 2\ H_2O + 2A^*$, where AH represents a reducing substrate and A* is a free radical product. The sequence of the reactions of HRP with aromatic substrates is characterized as a ping pong mechanism. The native peroxidase first reacts with hydrogen peroxide to form the oxidized enzyme intermediate compound I, which then can oxidize the reducing substrate (67). To react with the heme prosthetic group, H_2O_2 has to diffuse from the protein surface toward the heme pocket. It is proposed that hydrogen peroxide penetrates the protein matrix at a fluctuating entry point located between Phe-68 and Phe-142 and passes through a bottle-like channel to reach the heme iron (Fig. 8). Amino acid residues Phe-68 and Phe-142 are flanking the entry pore of the bottleneck, and their conformational fluctuations determine the accessibility of hydrogen peroxide to the interior (11). In comparing the two simulated models, the average distance between the backbones of Phe-68 and Phe-142 increases from 10.1 ± 1.6 Å in n-HRP to

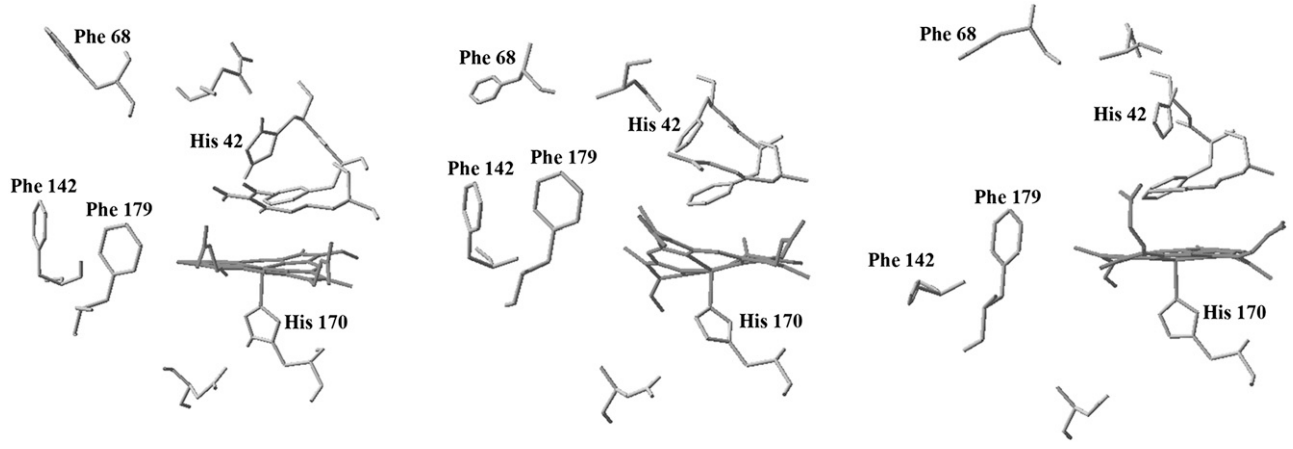

FIGURE 8 Structural features of the heme crevice in 1ATJ as the initial template (*left*) and in n-HRP (*middle*) and AQ-HRP (*right*) according to their MD average structures. Phe residues, 68, 142, and 179 guard the entrance to the exposed heme edge and control substrate access to the active site in HRP. Especially compare the distance between Phe-68 and Phe-142 in MD structures.

14.2 ± 0.8 Å in AQ-HRP (Fig. 8). Accordingly, the average distance between their side chains rises from 7.5 ± 1 Å to 12.8 ± 2 Å. These values indicate that the bottleneck entry is dilated as a result of AQ modification. Although such a structural change could facilitate diffusion of H_2O_2 molecules from the bulk solution to the active site inside the protein, the effect is expected to be less perceptible for small peroxides and remarkable for bulky ones.

In the proposed mechanism for the reaction of H_2O_2 with the active site of HRP two essential features are acid-base catalysis by the distal histidine (His-42) and charge stabilization of a precursor enzyme-substrate complex by the conserved distal arginine (Arg-38) (68). The histidine is thought to facilitate formation of the initial iron-peroxide complex by deprotonating the peroxide and subsequently promoting cleavage of the oxygen-oxygen bond by protonating the distal oxygen. Examination of the two models shows that the surface accessibility of this histidine in AQ-HRP (14.4 $Å^2$) is significantly higher than n-HRP (4.0 $Å^2$). This change could lead to enhanced reactivity of the modified enzyme to peroxide substrate.

Summing up the above simulation results the conclusion is reached that such conformational changes at the peroxide-binding site of HRP may contribute in reducing the K_m value of the enzyme upon modification (Table 1).

Aromatic substrate-binding sites

Substrate oxidation by HRP C occurs at the 'exposed' heme edge, a region comprising the heme methyl C18 and heme meso C20 protons (4). Spectroscopic and crystallographic studies have revealed a detailed picture of the site where aromatic substrates bind and react with the protein. A ring of three peripheral Phe residues, 68, 142, and 179, guard the entrance to the exposed heme edge (Fig. 8) (10). Amino acid residues Phe-68, Gly-69, Pro139, Ala-140, Pro-141, Phe-142, and Phe-179 are flanking the substrate access channel and together with the heme C20- and heme C18-methyl groups form the aromatic-binding pocket of HRP (2,10,12,14). Although in some cases hydrogen bonding between the reducing substrate and the active site residues of the distal heme pocket contribute to the stability of the substrate-HRP complex, most HRP substrates do not possess the potential to make such interactions and will therefore depend more on the hydrophobic interactions which characterize the peripheral region of the substrate channel of HRP (12).

As the values in Table 2 show, hydrophobic residues forming the substrate-binding pocket in HRP are generally more exposed in AQ-HRP, indicating that the hydrophobic patch functioning as a binding site or trap for reducing aromatic substrates is extended in the modified enzyme with respect to the native one. Consequently, the affinity of the aromatic substrates for the enzyme-active site is expected to increase after modification. Such structural changes may also contribute to the observed increases in the turnover number (k_{cat}) and catalytic efficiency of the enzyme upon modification.

TABLE 2 Accessible surface area ($Å^2$) of functionally important residues and groups

	n-HRP		AQ-HRP		
	Average	SD	Average	SD	Change
Heme	39.6	10.4	99.7	5.5	60.1
His-42	4.0	3.4	14.4	5.6	10.4
Phe-68	97.2	31.4	164.2	7.8	67.0
Gly-69	22.6	8.1	32.4	0.5	9.8
Trp-117	55.0	12.8	46.8	6.0	−8.2
Pro-139	7.3	6.4	21.7	7.1	14.4
Ala-140	6.3	5.5	33.8	8.7	27.5
Pro-141	9.1	5.7	21.3	6.7	12.2
Phe-142	105.9	14.1	91.6	2.1	−14.3
Phe-179	50.5	8.1	71.9	17.8	21.4

DISCUSSION

In this study, thermal denaturation and thermoinactivation investigations demonstrated that AQ modification enhances the conformational and operational stability of HRP. As pointed out in the introduction, several reports exist describing some improvement in thermostability of HRP after modification of its lysyl ε-amino groups using other modifiers (30–41). Ugarova et al. studied thermostability of HRP after modification of its lysyl amino groups with a variety of modifiers including anhydrides of monocarboxylic and dicarboxylic acids as well as picryl sulfonic acid (30), some of these compounds reversed the positive charge on the Lys, whereas others neutralized it. These studies showed that it is the degree of modification, rather than the nature of the modifier, which produces the major effect on the macromolecular conformation and the thermostability of the enzyme after modification. Using picryl sulfonic acid under relatively harsh conditions (40°C, pH 8.0), they modified all six HRP lysines. Activity was fully retained but stability at 56°C decreased by 30%. At 0°C, the identical procedure modified only three lysines but gave a threefold stabilization at 56°C. This suggests that HRP stability benefits from modification of three lysines, but the stabilizing effect is overcome as the modification proceeds to completion. Confirming this conclusion, most of the stabilized chemical derivatives of HRP reported to date have involved modifications of three lysines (30–41).

Ugarova et al. also observed that chemical modification of three amino groups decreases the intensity of the Soret band in CD spectra of HRP (30). Accordingly, they inferred that thermostability of the modified enzyme increases due to the decreased conformational mobility of the protein backbone around the heme. Similar changes in CD spectra of HRP after modification with maleic anhydride and citraconic anhydride has also been reported (41). Our Soret CD results provide additional support for this inference, but interestingly the near- and far-UV-CD as well as simulation studies indicate that this phenomenon is not limited to the heme pocket and the overall protein structure experiences a similar reduction in flexibility upon modification with AQ.

However, some authors have proposed another mechanism for the observed increase in conformational stability of HRP upon Lys modification (37,38,40). Based on their assumption, the Lys residues 174, 232, and 241 are the most probable sites for modification and the existing electrostatic repulsion between their positive charges in native HRP reduces the conformational stability of the enzyme. Thus, they believe that neutralization of these like charges upon modification lessens the tendency of the enzyme to unfold and so stabilizes HRP structure.

For several reasons, we believe that it is difficult to explain the observed stabilization solely based on charge neutralization. First, the Lys residues 174, 232, and 241 are exposed to the solvent, therefore, water molecules and dissolved ions shield the electrostatic interactions between their charged atoms reducing both their strength and distance over which they operate. Second, these lysines are located relatively far away from each other in the 3D structure of the enzyme (distances between the nitrogen centers of Lys-232–Lys-241, Lys-174–Lys-232, and Lys-174–Lys-241 in native HRP are 13.8, 19.4, and 18.38 Å, respectively), so their electrostatic fields cannot interact efficiently. Third, according to the HRP crystal structure (PDB code: 1ATJ), the neighboring charged amino acids whose charge centers are located within a radius of ~10 Å away from the ε-amino groups of Lys-174, Lys-232, and Lys-241 are Asp-29, Arg-31, Arg-75, Asp-220, Asp-222, Arg-224, Asp-230, Glu-238, and Glu-239. As seen, the negatively charged residues are predominant, signifying that the modified Lys residues are mainly engaged in attractive rather than repulsive electrostatic interactions. This suggests that any modification which neutralizes or reverses the charges of these lysines would be electrostatically unfavorable for protein stability.

In the case of our study, at first glance, modification increases the number of surface hydrophobic residues, whereas it reduces the number of surface-charged residues. So, one can expect the enzyme surface to be more hydrophobic after modification, but the experimental and simulation results disagree with this speculation. Extrinsic fluorescence studies using polarity-sensitive probes suggest a decrease in the total number of ANS/NR-binding sites upon modification. On the other hand, simulation results indicate that the overall size of the water-accessible hydrophobic area in native and modified HRP is more or less similar. Such differences between ANS/NR results and area estimation by MD simulation are expectable while considering that they apply different probes which significantly differ in size and molecular properties (in simulation, water is considered to be a small rigid sphere, whereas ANS and NR are bulky aromatic molecules). In this regard, a plausible explanation for the experimentally observed reduction in ANS/NR binding is the redistribution of the solvent-exposed hydrophobic area in AQ-HRP. As we pointed out previously, modification imposes new hydrophobic areas onto the protein surface through the Aql residues. Moreover, MD simulation indicates that hydrophobic residues forming the substrate-binding pocket in HRP are generally more exposed in AQ-HRP. In contrast, several other hydrophobic residues experience additional burial upon modification. Such redistribution of hydrophobic patches at the protein surface could affect the binding patterns of ANS and NR. However, avoiding complications, the above mentioned redistributions are generally consistent with the fact that extending the solvent-exposed hydrophobic area enhances the tendency of the protein structure to reduce the entropically unfavorable contact between the nonpolar portions of the protein surface and water. It means that although an increase in the surface area of hydrophobic clusters is an immediate consequence of the modification, the protein readjusts its structure to adapt to the new situation. So, some of the exposed hydrophobic clusters migrate from the surface to the protein interior. This rearrangement could also enhance the enthalpically favorable van der Waals packing interactions within the protein core (as confirmed by near-UV and Soret CD). This example clearly shows how manipulation of charge-hydrophobicity balance at the protein surface could induce remarkable changes within the protein interior.

Attachment of AQ relays also improves the catalytic properties of HRP. Although the changes are not large, they are significant. After modification, both the activity (V_{max} or k_{cat}) and enzyme-substrate affinity, $1/K_m$, have increased. Except for phthalic anhydride modification, to our knowledge, there is no report of any enhancement in HRP activity after Lys modification. It has been reported that phthalic anhydride modification of HRP marginally improves the catalytic activity but does not affect the K_m value (38). Again, no explanation has been presented for this observation. MD simulations on native and AQ-HRP showed substantial differences between the two structures particularly in the peroxide and aromatic substrate-binding sites. Comparing the peroxide-binding sites, dilated penetration channel, and more accessible binding site in AQ-HRP reflects higher reactivity of the enzyme to the peroxide substrates. The aromatic-binding site of AQ-HRP also benefits from a more extended hydrophobic trap and more exposed heme reactive edge, suggesting enhanced reactivity to the reducing substrates.

In conclusion, evaluation of the experimental and simulation studies, both from this and our previous work (44), demonstrates that the simple approach of AQ modification produces a novel derivative of HRP with enhanced electron transfer properties, catalytic efficiency, and stability for biotechnological applications. Moreover, the experimental and simulation findings presented here may provide new insights into how manipulation of the charge/hydrophobicity balance at the protein surface could affect the protein structure and function.

The authors thank Dr. Khosro Khajeh (Tarbiat Modarres University, Tehran, Iran), Dr. Hamid Mobasheri (University of Tehran, Tehran, Iran), and Dr. Homayoon Khalili (IBM) for their useful comments.

Financial support provided by the Research Council of the University of Tehran is gratefully appreciated.

REFERENCES

1. Dunford, H. B. 1991. Horseradish peroxidases: structure and kinetic properties. *In* Peroxidases in Chemistry and Biology. I. K. E. Everse and M. B. Grisham, editors. CRC Press/Boca Raton, FL. 1–24.
2. Nigel, C. V. 2004. Horseradish peroxidase: a modern view of a classic enzyme. *Phytochemistry.* 65:249–259.
3. Berglund, G. I., G. H. Carlsson, A. T. Smith, H. Szöke, A. Henriksen, and J. Hajdu. 2002. The catalytic pathway of horseradish peroxidase at high resolution. *Nature.* 417:463–468.
4. Welinder, K. G. 1985. Plant peroxidases. Their primary, secondary and tertiary structures and relation to cytochrome *c* peroxidase. *Eur. J. Biochem.* 151:497–504.
5. Welinder, K. G. 1979. Amino acid sequence studies of horseradish peroxidase. *Eur. J. Biochem.* 95:483–502.
6. Smith, A. T., N. Santama, M. Edwards, R. C. Bray, R. N. F. Thomeley, and J. F. Burke. 1990. Expression of a synthetic gene for horseradish peroxidase C in *Escherichia coli* and folding and activation of the recombinant enzyme with Ca^{2+} and heme. *J. Biol. Chem.* 265:13335–13343.
7. Welinder, K. G. 1976. Covalent structure of the glycoprotein horseradish peroxidase. *FEBS Lett.* 72:19–23.
8. Clarke, J., and L. M. Shannon. 1976. The isolation and characterization of the glycopeptides from horseradish peroxidase isoenzymes C. *Biochim. Biophys. Acta.* 421:428–442.
9. Yang, B. Y., J. S. S. Gray, and R. Montgomery. 1996. The glycans of horseradish peroxidase. *Carbohydr. Res.* 287:203–212.
10. Gajhede, M., D. J. Schuller, A. Henriksen, A. T. Smith, and T. L. Poulos. 1997. Crystal structure of horseradish peroxidase C at 2.15 angstrom resolution. *Nat. Struct. Biol.* 4:1032–1038.
11. Khajehpour, M., I. Rietveld, S. Vinogradov, N. V. Prabhu, K. A. Sharp, and J. M. Vanderkooi. 2003. Accessibility of oxygen with respect to the heme pocket in horseradish peroxidase. *Proteins Struct. Funct. Genet.* 53:656–666.
12. Henriksen, A., D. J. Schuller, K. Meno, K. G. Welinder, A. T. Smith, and M. Gajhede. 1998. Structural interactions between horseradish peroxidase C and the substrate benzhydroxamic acid determined by x-ray crystallography. *Biochemistry.* 37:8054–8060.
13. Filizola, M., and G. H. Loew. 2000. Role of protein environment in horseradish peroxidase compound I formation: molecular dynamics simulations of horseradish peroxidase–HOOH complex. *J. Am. Chem. Soc.* 122:18–25.
14. Henriksen, A., A. T. Smith, and M. Gajhede. 1999. The structures of the horseradish peroxidase C-ferulic acid complex and the ternary complex with cyanide suggest how peroxidases oxidize small phenolic substrates. *J. Biol. Chem.* 274:35005–35011.
15. Carlsson, G. H., P. Nicholls, D. Svistunenko, G. I. Berglund, and J. Hajdu. 2005. Complexes of horseradish peroxidase with formate, acetate, and carbon monoxide. *Biochemistry.* 44:635–642.
16. Laberge, M., S. Osvath, and J. Fidy. 2001. Aromatic substrate specificity of horseradish peroxidase C studied by a combined fluorescence line narrowing/energy minimization approach: the effect of localized side-chain reorganization. *Biochemistry.* 40:9226–9237.
17. Ziemys, A., and J. Kulys. 2005. Heme peroxidase clothing and inhibition with polyphenolic substances revealed by molecular modeling. *Comput. Biol. Chem.* 29:83–90.
18. Rodríguez-López, J. N., D. J. Lowe, J. Hernández-Ruiz, A. N. P. Hiner, F. García-Cánovas, and R. N. F. Thorneley. 2001. Mechanism of reaction of hydrogen peroxide with horseradish peroxidase: identification of intermediates in the catalytic cycle. *J. Am. Chem. Soc.* 123: 11838–11847.
19. Kaposi, A. D., N. V. Prabhu, S. D. Dalosto, K. A. Sharp, W. W. Wright, S. S. Stavrov, and J. M. Vanderkooi. 2003. Solvent dependent and independent motions of CO–horseradish peroxidase examined by infrared spectroscopy and molecular dynamics calculations. *Biophys. Chem.* 106:1–14.
20. Howes, B. D., A. Feis, L. Raimondi, C. Indiani, and G. Smulevich. 2001. The critical role of the proximal calcium ion in the structural properties of horseradish peroxidase. *J. Biol. Chem.* 276:40704–40711.
21. Laberge, M., Q. Huang, R. Schweitzer-Stenner, and J. Fidy. 2003. The endogenous calcium ions of horseradish peroxidase C are required to maintain the functional nonplanarity of the heme. *Biophys. J.* 84:2542–2552.
22. Newmyer, S. L., and P. R. Ortiz de Montellano. 1995. Horseradish peroxidase His42Ala, His42Val, and Phe41Ala mutants: histidine catalysis and control of substrate access to the heme iron. *J. Biol. Chem.* 270:19430–19438.
23. Rodriguez-Lopez, J. N., A. T. Smith, and R. N. F. Thorneley. 1996. Role of arginine 38 in horseradish peroxidase: a critical residue for substrate binding and catalysis. *J. Biol. Chem.* 271:4023–4030.
24. Ator, M., and P. R. Ortiz de Montellano. 1987. Protein control of prosthetic heme reactivity. Reaction of substrates with the heme edge of horseradish peroxidase. *J. Biol. Chem.* 262:1542–1551.
25. Azevedo, A. M., V. C. Martins, D. M. F. Prazeres, V. Vojinovic, J. M. S. Cabral, and L. P. Fonseca. 2003. Horseradish peroxidase: a valuable tool in biotechnology. *Biotech. Ann. Rev.* 9:199–247.
26. Moreno, J. M., and C. Ó. Fágáin. 1997. Activity and stability of native and modified alanine aminotransferase in cosolvent systems and denaturants. *J. Mol. Catal. B Enzym.* 2:271–279.
27. Khajeh, K., H. Naderi-Manesh, B. Ranjbar, A. A. Moosavi-Movahedi, and M. Nemat-Gorgani. 2001. Chemical modification of lysine residues in *Bacillus* α-amylases: effect on activity and stability. *Enzyme Microb. Technol.* 28:543–549.
28. Murphy, A., and C. Ó. Fágáin. 1998. Chemically stabilized trypsin used in dipeptide synthesis. *Biotechnol. Bioeng.* 58:366–373.
29. Mozhaev, V. V., V. A. Šikšnis, N. S. Melik-Nubarov, N. Z. Galkantaite, G. J. Denis, E. P. Butkus, B. Y. Zaslavsky, N. M. Mestechkina, and K. Martinek. 1988. Protein stabilization via hydrophilization: covalent modification of trypsin and α-chymotrypsin. *Eur. J. Biochem.* 173:147–154.
30. Ugarova, N. N., G. D. Rozhkova, and I. V. Berezin. 1979. Chemical modification of the ε-amino groups of lysine residues in horseradish peroxidase and its effect on the catalytic properties and thermostability of the enzyme. *Biochim. Biophys. Acta.* 570:31–42.
31. Ryan, O., M. R. Smyth, and C. Ó. Fágáin. 1994. Thermostabilized chemical derivatives of horseradish peroxidase. *Enzyme Microb. Technol.* 16: 501–505.
32. Miland, E., M. R. Smyth, and C. Ó. Fágáin. 1996. Modification of horseradish peroxidase with bifunctional *N*-hydroxysuccinimide esters: effects on molecular stability. *Enzyme Microb. Technol.* 19:242–249.
33. O'Brien, A. M., and C. Ó. Fágáin. 1996. Chemical stabilization of recombinant horseradish peroxidase. *Biotechnol. Tech.* 10:905–910.
34. Miland, E., M. R. Smyth, and C. Ó. Fágáin. 1996. Increased thermal and solvent tolerance of acetylated horseradish peroxidase. *Enzyme Microb. Technol.* 19:63–67.
35. O'Brien, A. M. 1997. Chemical modification and characterization of horseradish peroxidase and its derivatives for environmental applications. PhD thesis. Dublin City University, Ireland.
36. Garcia, D., F. Ortéga, and J. L. Marty. 1998. Kinetics of thermal inactivation of horseradish peroxidase: stabilizing effect of methoxypoly(ethylene glycol). *Biotechnol. Appl. Biochem.* 27:49–54.
37. O'Brien, A. M., C. Ó. Fágáin, P. F. Nielsen, and K. G. Welinder. 2001. Location of crosslinks in chemically stabilized horseradish peroxidase. Implications for design of crosslinks. *Biotechnol. Bioeng.* 76:277–284.
38. O'Brien, A. M., A. T. Smith, and C. Ó. Fágáin. 2003. Effects of phthalic anhydride modification on horseradish peroxidase stability and activity. *Biotechnol. Bioeng.* 81:233–240.
39. Song, H. Y., J. Z. Liu, Y. H. Xiong, L. P. Weng, and L. N. Ji. 2003. Treatment of aqueous chlorophenol by phthalic anhydride-modified horseradish peroxidase. *J. Mol. Catal. B Enzym.* 22:37–44.
40. Hassani, L., B. Ranjbar, K. Khajeh, H. Naderi-Manesh, M. Naderi-Manesh, and M. Sadeghi. 2006. Horseradish peroxidase thermostabilization: the combinatorial effects of the surface modification and the polyols. *Enzyme Microb. Technol.* 38:118–125.

41. Liu, J. Z., T. L. Wang, M. T. Huang, H. Y. Song, L. P. Weng, and L. N. Ji. 2006. Increased thermal and organic solvent tolerance of modified horseradish peroxidase. *Protein Eng. Des. Sel.* 19:169–173.

42. Urrutigoity, M., M. Baboulene, and A. Lattes. 1991. Use of pyrocarbonates for chemical modification of histidine residues of horseradish peroxidase. *Bioorg. Chem.* 19:66–76.

43. Hahn, M. E., and T. W. Muir. 2005. Manipulating proteins with chemistry: a cross-section of chemical biology. *Trends Biochem. Sci.* 30:26–34.

44. Mogharrab, N., and H. Ghourchian. 2005. Anthraquinone 2-carboxylic acid as an electron shuttling mediator and attached electron relay for horseradish peroxidase. *Electrochem. Commun.* 7:466–471.

45. Bradford, M. 1976. A rapid and sensitive method for the quantitation of microgram quantities of protein utilizing the principle of protein-dye binding. *Anal. Biochem.* 72:248–254.

46. Habeeb, A. S. F. A. 1966. Determination of free amino groups in proteins by trinitrobenzenesulfonic acid. *Anal. Biochem.* 14:328–336.

47. Bubnis, W., and C. Ofner. 1992. The determination of ε-amino groups in soluble and poorly soluble proteinaceous materials by a spectrophotometric method using trinitrobenzenesulfonic acid. *Anal. Biochem.* 297:129–133.

48. Worthington, C. C. 1988. The Worthington Manual. Worthington Biochemical, Lakewood, NJ.

49. Lonhienne, T., C. Gerday, and G. Feller. 2000. Psychrophilic enzymes: revisiting the thermodynamic parameters of activation may explain local flexibility. *Biochim. Biophys. Acta.* 1543:1–10.

50. Berendsen, H. J. C., D. van der Spoel, and R. van Drunen. 1995. GROMACS: a message-passing parallel molecular dynamics implementation. *Comput. Phys. Commun.* 91:43–56.

51. Lindahl, E., B. Hess, and D. van der Spoel. 2001. GROMACS 3.0: a package for molecular simulation and trajectory analysis. *J. Mol. Model.* 7:306–317.

52. van der Spoel, D., E. Lindahl, B. Hess, G. Groenhof, A. E. Mark, and H. J. C. Berendsen. 2005. GROMACS: fast, flexible and free. *J. Comput. Chem.* 26:1701–1718.

53. The Dundee PRODRG2 Server. http://davapc1.bioch.dundee.ac.uk/programs/prodrg/

54. Schuettelkopf, A. W., and D. M. F. van Aalten. 2004. PRODRG: a tool for high-throughput crystallography of protein-ligand complexes. *Acta Crystallogr. Sect. D-Biol. Crystallogr.* 60:1355–1363.

55. Berendsen, H. J. C., J. P. M. Postma, W. F. van Gunsteren, A. Di Nola, and J. R. Haak. 1984. Molecular dynamics with coupling to an external bath. *J. Chem. Phys.* 81:3684–3690.

56. Hess, B., H. Bekker, H. J. C. Berendsen, and J. G. E. M. Fraaije. 1997. LINCS: a linear constraint solver for molecular simulations. *J. Comput. Chem.* 18:1463–1472.

57. Darden, T., D. York, and L. Pedersen. 1993. Particle mesh Ewald: an N Log (N) method for Ewald sums in large systems. *J. Chem. Phys.* 98: 1463–1472.

58. Hoare, D., and D. E. Koshland. 1967. A method for the quantitative modification and estimation of carboxylic acid groups in proteins. *J. Biol. Chem.* 242:2447–2453.

59. Vilmos Kertesz, V., N. A. Whittemore, G. B. Inamati, M. Manoharan, P. D. Cook, D. C. Baker, and J. Q. Chambers. 2000. Electrochemical detection of surface hybridization of oligodeoxynucleotides bearing anthraquinone tags at gold electrodes. *Electroanal.* 12:589–594.

60. Pina, D. G., A. V. Shnyrova, F. Gavilanes, A. Rodríguez, F. Leal, M. G. Roig, I. Y. Sakharov, G. G. Zhadan, E. Villar, and V. L. Shnyrov. 2001. Thermally induced conformational changes in horseradish peroxidase. *Eur. J. Biochem.* 268:120–126.

61. Kelly, S. M., and N. C. Price. 2000. The use of circular dichroism in the investigation of protein structure and function. *Curr. Protein Pept. Sci.* 1:349–384.

62. Gabbianelli, R., G. Zolese, E. Bertoli, and G. Falcioni. 2004. Correlation between functional and structural changes of reduced and oxidized trout hemoglobins I and IV at different pHs. A circular dichroism study. *Eur. J. Biochem.* 271:1971–1979.

63. Blauer, G., N. Sreerama, and R. W. Woody. 1993. Optical activity of hemoproteins in the Soret region: circular dichroism of the heme undecapeptide of cytochrome *c* in aqueous solution. *Biochemistry.* 32: 6674–6679.

64. Matulis, D., and R. Lovrien. 1998. 1-Anilino-8-naphthalene sulfonate anion-protein binding depends primarily on ion pair formation. *Biophys. J.* 74:422–429.

65. Sackett, D. L., and J. Wolff. 1987. Nile red as a polarity-sensitive fluorescent probe of hydrophobic protein surfaces. *Anal. Biochem.* 167: 228–234.

66. Copeland, R. A. 2000. Enzymes: A Practical Introduction to Structure, Mechanism, and Data Analysis. John Wiley & Sons, New York.

67. Kedderis, G. L., and P. F. Hollenberg. 1983. Characterization of the *N*-demethylation reactions catalyzed by horseradish peroxidase. *J. Biol. Chem.* 258:8129–8138.

68. Poulos, T. L., and J. Kraut. 1980. The stereochemistry of peroxidase catalysis. *J. Biol. Chem.* 255:8199–8205.